Article

Title: Channelized melt flow in downwelling mantle: Implications for 226Ra-210Pb disequilibria in arc magmas

Creators: Petford, N., Koenders, M. A. and Turner, S.

DOI: 10.1029/2007JB005563

Example citation: Petford, N., Koenders, M. A. and Turner, S. (2008) Channelized melt flow in downwelling mantle: Implications for 226Ra-210Pb disequilibria in arc magmas. *Journal of Geophysical Research: Solid Earth.* **113**(B11202) 2169-9356.

Version: Published version

Official URL: http://dx.doi.org/10.1029/2007JB005563

Channelized melt flow in downwelling mantle: Implications for ^{226}Ra-^{210}Pb disequilibria in arc magmas

N. Petford,[1] M. A. Koenders,[2] and S. Turner[3]

[1]   We present the results of an analytical model of porous flow of viscous melt into a steadily dilating "channel" (defined as a cluster of smaller veins) in downwelling subarc mantle. The model predicts the pressure drop in the mantle wedge matrix surrounding the channel needed to drive melt flow as a function of position and time. Melt is sucked toward the dilatant region at a near-constant velocity (10^{-5} s^{-1}) until veins comprising the channel stop opening ($t = \tau$). Fluid elements that complete their journey within the time span $t < \tau$ arrive at a channel. Our results make it possible to calculate the region of influence sampled by melt that surrounds the channel. This region is large compared to the model size of the channelized region driving flow. For a baseline dilation time of 1 year and channel half width of 2 m, melt can be sampled over an 80-m radius and has the opportunity to sample matrix material with potentially contrasting chemistry on geologically short timescales. Our mechanical results are consistent with a downgoing arc mantle wedge source region where melting and melt extraction by porous flow to a channel network are sufficiently rapid to preserve source-derived ^{238}U-^{230}Th-^{226}Ra, and potentially also ^{226}Ra-^{210}Pb, disequilibria, prior to magma ascent to the surface. Since this is the rate-determining step in the overall process, it allows the possibility that such short-lived disequilibria measured in arc rocks at the surface are derived from deep in the mantle wedge. Stresses due to partial melting do not appear capable of producing the desired sucking effect, while the order of magnitude rate of shear required to drive dilation of $\sim 10^{-7}$ s^{-1} is much larger than values resulting from steady state subduction. We conclude that local deformation rates in excess of background plate tectonic rates are needed to "switch on" the dilatant channel network and to initiate the sucking effect.

1.   Introduction

[2]   The dynamic behavior of the Earth is a result of its internal heat. Volcanism provides the most spectacular manifestation of this, and heat advection by magmas is the most efficient means of heat transport. Beneath the Earth's volcanic mid-ocean ridges and oceanic islands, melting occurs in an upwelling mantle matrix with melt extraction often presumed to occur via percolative flow followed by channeled flow [e.g., *Spiegelman et al.*, 2001; *Spiegelman and Kelemen*, 2003]. Currently, the timescales and length scales governing this important flow transition are poorly known. Yet without some estimate of melt velocities and transport times, the degree to which interaction between melt and peridotite matrix may take place remains speculative at best. U series disequilibria can be used to constrain the rate of matrix upwelling and also the threshold porosity at which melt is extracted from the matrix. In contrast, the total time for melt extraction is ambiguous depending on whether the observed disequilibria are modeled by dynamic melting with rapid extraction [e.g., *McKenzie*, 1985; *Williams and Gill*, 1989] or equilibrium porous flow involving very slow melt percolation [*Spiegelman and Elliott*, 1993; *Asimow and Stolper*, 1999]. Because the exact melting rate and porosity are linked to the total time involved, better knowledge of the timescales and length scales of melt transport in the source region would help improve estimates of these variables. Nevertheless, there is growing evidence that melt extraction beneath ridges and ocean island volcanoes is fast and may in some cases take place on decadal timescales [*Bourdon et al.*, 2005; *Rubin et al.*, 2005a; *Stracke et al.*, 2006].

[3]   At island arcs the situation is rather different. Because of induced convection against the subducting plate, most current models of melt production in arcs assume that the mantle wedge directly above the slab, where a significant portion of arc magmas is generated, moves downward through the melting zone. Furthermore, the ^{231}Pa disequilibria are consistent with the matrix flow rate in the melting region being the same as the local convergence rates

---

[1]School of Conservation Sciences, Bournemouth University, Poole, UK.
[2]Centre for Earth and Environmental Science Research, Kingston University, Kingston, UK.
[3]GEMOC, Department of Earth and Planetary Sciences, Macquarie University, Sydney, New South Wales, Australia.
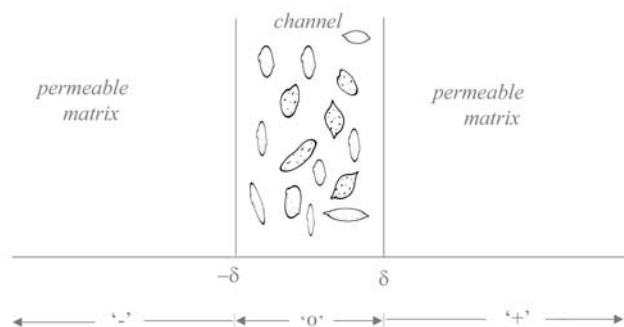
Figure 1. Geometry of the channel, defined as a high-porosity dilational zone comprising numerous smaller veins. Three regions are identified: 0, where the dilation occurs; plus, almost undeformable permeable material to the right of 0 at $x > \delta$; and minus, almost undeformable permeable material to the left of 0 at $x < -\delta$.

[*Turner et al.*, 2006; *Huang and Lundstrom*, 2007]. Although recent work suggests that decompression melting due to viscous entrainment may also take place in some arcs [*Conder et al.*, 2002], the problem of melt extraction in a downwelling matrix still requires attention. Additionally, ^{226}Ra excesses in arc lavas correlate with trace element indices of fluid addition (e.g., Sr/Th) and so are inferred to result from fluid addition from the subducting plate. Critically, because this implies these signals originate at the base of the melt region, their preservation allows important constraints to be placed on the magma extraction rate, and this may be on the order of $100-1000$ m a^{-1} [*Turner et al.*, 2001]. Although porous flow models can also produce large ^{226}Ra excesses [*Spiegelman and Elliott*, 1993], they do not predict a positive correlation with Sr/Th.

[4] In contrast to creeping flow modeled successfully for mid-ocean ridges, these higher transport rates require channel-dominated melt ascent toward the surface. However, an important condition remains, namely, that the melt is supplied to channels over some governing length scale fast enough that short-lived isotope disequilibria are preserved. Such high rates require a fluid dynamical explanation, yet they appear incompatible with a transport process governed purely by compaction and simple porous flow [e.g., *Sleep*, 1988; *Stevenson*, 1989; *Maaloe*, 2005].

[5] Clearly, there is a need to develop physical models for melt transport in the mantle wedge above a subducting slab analogous to those put forward for melt extraction at mid-ocean ridges [e.g., *Aharonov et al.*, 1995; *Spiegelman et al.*, 2001; *Spiegelman and Kelemen*, 2003], whereby an initially small melt fraction, distributed at or along grain boundaries, develops into a channelized network. More generally, in order to develop a self-consistent model of subduction zones, there is a need to explore physical processes that take place in the mantle wedge on short temporal and spatial scales [e.g., *van Keken*, 2003]. As a first step toward this goal, we present the initial results of an analytical study of melt flow in porous, downwelling arc mantle. We assume a simple 1-D geometry where melt flows radially toward a zone of reduced pressure, defined macroscopically as a linear channel of constant half width bounding a cluster of smaller veins that open incrementally over a fixed timescale.

From this, we seek as a first step to establish a rigorous solution to the mechanics of the problem and provide order of magnitude estimates of (1) the characteristic pressure gradients needed to drive porous flow of melt toward a dilating channel, (2) the maximum distance (or radius of influence) surrounding a dilating channel from which melt can be sampled such that a required activity ratio is preserved, and (3) the possible mechanism(s) governing dilation in downwelling mantle. Once the theory part is established, the way is paved for further (numerical) work that can model the flow process in more detail.

2. Model Geometry and Assumptions

[6] The majority of U series evidence to date points to the need for some kind of channelized flow in the mantle [e.g., *McKenzie*, 1985; *Turner et al.*, 2001, 2003; *Stracke et al.*, 2006]. Yet despite this, some element of porous flow must still prevail at the outset of the transport process [e.g., *Spiegelman et al.*, 2001]. Our goal at this stage is not to model channel formation itself but rather to show under what conditions melt flow will be fast enough to preserve isotopic disequilibrium in the source region (note we use "channel" here to describe some form of linear, dilatant feature as distinct from a brittle crack).

[7] A sketch of the simple geometry under investigation is shown in Figure 1. The model comprises a central region (or channel) that contains dilational structures or veins (for want of a better word). The half width of the channel δ is of the order of meters (we use a guideline number of $\delta = 2$ m in our calculations), comparable with estimates from *Takahashi* [1992] of vein and channel structures in mantle rocks now preserved at the surface. The permeability in the dilating channel is much greater than that of the surrounding rock. In order to estimate its value, we employ the well-known Kozeny-Carman formula, which is normally used for granular materials. Let the length scale d between the veins comprising the channel be of the order of 10^{-2} m and the melt fraction (porosity) $n_0 = 0.2$, then the permeability in the region that is dominated by the vein system comes out as $\kappa_0 = d^2 n_0^3 / [150(1 - n_0)^3] \simeq 10^{-8}$ m^2; this value will be fixed arbitrarily as a guideline number to allow us to focus on the details of the process. The channel is surrounded by mantle with fixed lower permeability: $\kappa = 10^{-14}$ m^2. The conductivities in the channel and surrounding rock related to the permeabilities through the viscosity η are $k_0 = \kappa_0/\eta$ and $k = \kappa/\eta$.

3. Flow Equations

[8] The melt density and viscosity remain constant during flow. We solve for the average pressure drop in the channel and recover the associated flow rate as melt is sucked toward it. Three regions are identified (Figure 1): "zero," where the channel is located; "plus," almost undeformable permeable material to the right of 0 at $x > \delta$; and "minus," almost undeformable permeable material to the left of 0 at $x < -\delta$. The flow is driven by a strain that is ramped up to a value e_0 in a time τ. For $t > \tau$ the strain is kept constant at e_0. The magma is compressible with compressibility β; the porosities are n_0 in the channel and n in the surrounding rock. The fluid excess pressure is denoted by p.

Table 1. Values and Constants Used in the Analytical Model

Process	Symbol	Value	Unit
Channel opening volume strain	e_0	0.1	-
Melt viscosity	η	1.0	Pa s
Permeability of the channel region	k_0	10^{-8}	Pa^{-1} m^2 s^{-1}
Matrix permeability	k	10^{-12}	Pa^{-1} m^2 s^{-1}
Melt compressibility	β	10^{-10}	Pa^{-1}
Shear strain in the zero region	γ	10^{-7}	s^{-1}
Porosity of the channel region	n_0	0.2	-
Matrix porosity (melt fraction)	n	0.001	-
Half width of the channel region	δ	2	m
Channel opening time	τ	10^7	s

[9] Biot's equation reads

$$k_0 \frac{\partial^2 p}{\partial x^2} = n_0 \beta \frac{\partial p}{\partial t} + \frac{\partial e}{\partial t} \quad (-\delta < x < \delta) \tag{1}$$

$$k \frac{\partial^2 p}{\partial x^2} = n\beta \frac{\partial p}{\partial t} \quad (x > \delta, \ x < -\delta). \tag{2}$$

[10] The boundary conditions are

$$p(\delta - \varepsilon, t) = p(\delta + \varepsilon, t) \quad (\varepsilon \to 0), \tag{3}$$

$$p(-\delta - \varepsilon, t) = p(-\delta + \varepsilon, t) \quad (\varepsilon \to 0), \tag{4}$$

$$k_0 \frac{\partial p}{\partial x}(\delta - \varepsilon, t) = k \frac{\partial p}{\partial x}(\delta + \varepsilon, t)(\varepsilon \to 0), \tag{5}$$

$$k_0 \frac{\partial p}{\partial x}(-\delta + \varepsilon, t) = k \frac{\partial p}{\partial x}(-\delta - \varepsilon, t) \quad (\varepsilon \to 0), \tag{6}$$

$$\frac{\partial p}{\partial x}(\pm L, t) = 0 \quad (L \to \infty). \tag{7}$$

[11] The solution is obtained by Laplace transform. Full details are given in Appendix A. The solution of the problem is given in terms of functions $\Psi_0(\zeta, t)$ and $\Psi_1(\zeta, t)$; these depend on the time it takes for the veins to open (τ). In Appendix A, their form is derived

$$\Psi_0(\zeta, t) = -\frac{\zeta \sqrt{t} \exp\left(-\frac{\zeta^2}{4t}\right)}{\tau \sqrt{\pi}}$$
$$+ \frac{(2t + \zeta^2)\left[1 - \mathrm{erf}\left(\frac{\zeta}{2\sqrt{t}}\right)\right]}{2\tau} \quad (t < \tau)$$
$$= 1 + \frac{\zeta \left(\exp\left(\frac{-\zeta^2}{4(t-\tau)}\right)\sqrt{t-\tau} - \exp\left(\frac{-\zeta^2}{4t}\right)\sqrt{t}\right)}{\tau\sqrt{\pi}}$$
$$\cdot \frac{(2t - 2\tau + \zeta^2)\mathrm{erf}\left(\frac{\zeta}{2\sqrt{t-\tau}}\right) - (2t + \zeta^2)\mathrm{erf}\left(\frac{\zeta}{2\sqrt{t}}\right)}{2\tau}$$
$$\cdot (t > \tau) \tag{8}$$

$$\Psi_1(\zeta, t) = \frac{2\sqrt{t}\exp\left(-\frac{\zeta^2}{4t}\right)}{\tau\sqrt{\pi}} - \frac{\zeta\left[1 - \mathrm{erf}\left(\frac{\zeta}{2\sqrt{t}}\right)\right]}{\tau} \quad (t < \tau)$$
$$= -\frac{2\left(\exp\left(\frac{-\zeta^2}{4(t-\tau)}\right)\sqrt{t-\tau} - \exp\left(\frac{-\zeta^2}{4t}\right)\sqrt{t}\right)}{\tau\sqrt{\pi}}$$
$$- \frac{\zeta\left[\mathrm{erf}\left(\frac{\zeta}{2\sqrt{t-\tau}}\right) - \mathrm{erf}\left(\frac{\zeta}{2\sqrt{t}}\right)\right]}{\tau} \quad (t > \tau). \tag{9}$$

[12] The superficial velocity (that is, the fluid discharge per unit time and area) of melt flowing toward the channel is simply

$$v = -k \frac{\partial p}{\partial x}. \tag{10}$$

[13] For convenience, two parameters with the dimension of $\sqrt{s}$ m^{-1} are introduced: $\mu_0 = \sqrt{n_0\beta/k_0}$ and $\mu = \sqrt{n\beta/k}$. The pore pressure (as a function of position and time) due to the opening vein in the region marked plus is

$$p(x, t) = \frac{e_0 k_0 \mu_0}{\beta n_0 (k\mu + k_0\mu_0)} \sum_{j=0}^{\infty} \left(\frac{-k\mu + k_0\mu_0}{k\mu + k_0\mu_0}\right)^j$$
$$\cdot [\Psi_0(\mu(x - \delta) + 2(j+1)\mu_0\delta, t)$$
$$- \Psi_0(\mu(x - \delta) + 2j\mu_0\delta, t)], \tag{11}$$

and the superficial velocity turns out to be

$$v(x, t) = -\frac{e_0 k k_0 \mu_0 \mu}{\beta n_0 (k\mu + k_0\mu_0)} \sum_{j=0}^{\infty} \left(\frac{-k\mu + k_0\mu_0}{k\mu + k_0\mu_0}\right)^j$$
$$\cdot [\Psi_1(\mu(x - \delta) + 2(j+1)\mu_0\delta, t)$$
$$- \Psi_1(\mu(x - \delta) + 2j\mu_0\delta, t)]. \tag{12}$$

[14] The corresponding actual melt velocity is $v(x, t)/n$.

4. Results

[15] Our primary aim here is to model the magnitude of melt flow in response to pressure reductions associated with the opening up of channels as defined in Figure 1 in the mantle wedge (how the channels themselves might happen to form is discussed in section 5). There is no simple scaling in this problem as there are three length scales: $\lambda_1 = \mu_0^{-1}\sqrt{\tau}$, $\lambda_2 = \mu^{-1}\sqrt{\tau}$, and $\lambda_3 = \delta$. The times scales to τ as well as to the factors $\beta n_0(k\mu + k_0\mu_0)/(e_0 k k_0\mu_0\mu\lambda_i)$ ($i = 1,2,3$). So, here it is important to have some idea of the variable range for results to be presented. Naturally, there is an element of speculation in the parameter values as no precise measurements are available. In our simple model we take τ (dilation time) as 1 year. This is arbitrary. Any other value of τ is, of course, permitted; examples include scaling the channel opening time to a short-lived isotope half-life. Relevant values are summarized in Table 1. To begin with, the pressure as a function of position and time is obtained. This is illustrated here for a choice of parameters (melt viscosity, melt fraction, etc.) as given in Table 1 with the exception of k, which is set to 10^{-10} Pa^{-1} m^2 s^{-1}; the reason for the deviation of the permeability parameter is that this choice results in rather smoother curves, which are desirable for
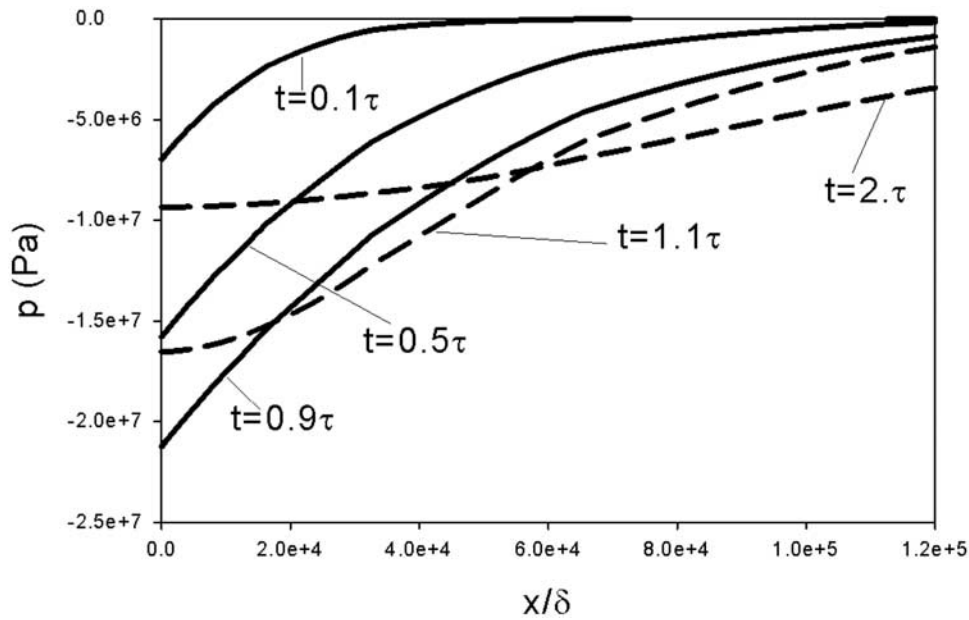
Figure 2. Pressure as a function of nondimensional position at various times (t). All parameters are as in Table 1 except $k = 10^{-10}$ Pa^{-1} m^2 s^{-1}. Solid lines show the pressure history as the channel is opening ($t < \tau$) and dashed lines show the pressure history where $t > \tau$. The behavior is such that after a short time the pressure settles back to a value close to initial. The pressure drop is, however, active over a wide area.

illustrative purposes. Figure 2 shows the pressure as a function of position in the plus region, plotted as a function of position (expressed in δ) at various times. It is seen that the pressure falls as the channels open up (a good analogy is that of drawing fluid into a syringe at a fixed rate) and that the region of influence is large compared to the size of the

channelized region. When the channel opening ceases (at $t = \tau$), the pressure rapidly returns to the equilibrium value $p = 0$ while the magnitude of the pressure gradient (and, thus, the fluid velocity) decreases. In the example here, the gradient is already negligible after $t = 2\tau$. This behavior is exactly as one would expect it. The question is, however,
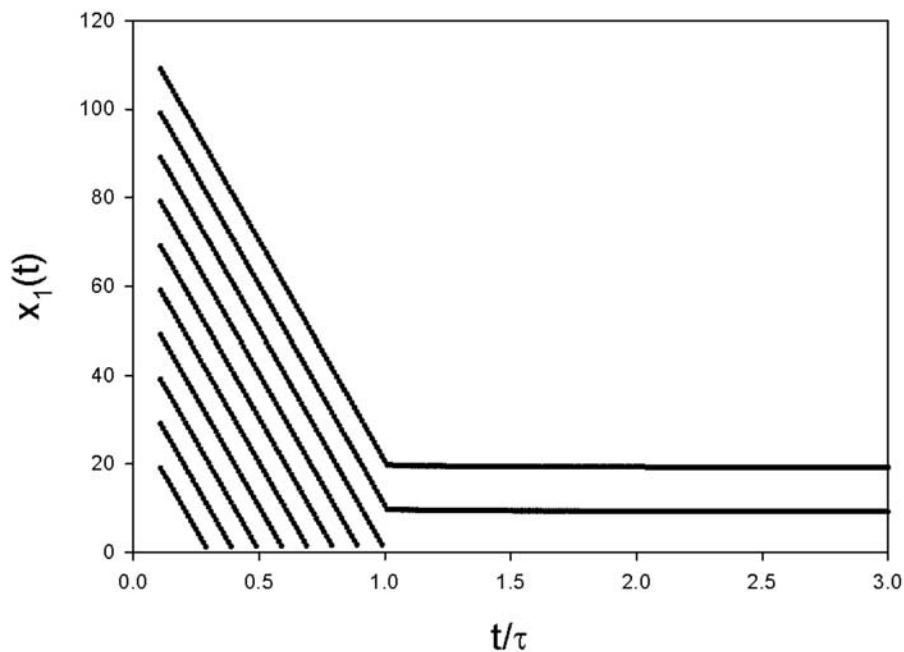

Figure 3. Trajectories of fluid elements for the parameter values in the Table 1. Melt is drawn toward the opening channel by pressure gradients set up as the channel widens over the period of 1 year, after which the pressure gradient is shut off. The channel is located at position $t/\tau = 1.0$. Fluid will reach this position from a distance $x_1(t)$ of up to 80 m away.
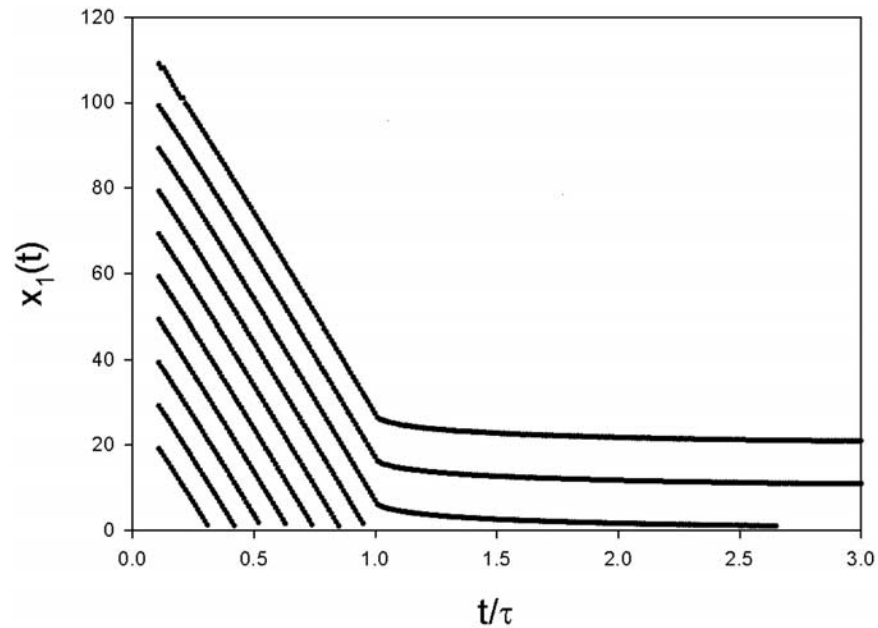
Figure 4. The same calculation as shown in Figure 3 but where the melt phase is slightly compressible (due, for example, to the presence of dissolved gas). This small but significant effect results in some degree of flow relaxation even after sucking has stopped. For example, calculated fluid trajectories in excess of 80 m distance can reach the channel but on a timescale slightly greater than $t/\tau = 2.6$.

how far will a fluid element travel in the process? To answer this question, trajectories are calculated. The actual fluid velocity in the plus region is $v(x,t)/n$, and, therefore, the location x_1 of a fluid element at time t that was initially at x_0 is

$$x_1(t) = x_0 + \int_0^t v(x_1(\bar{t}), \bar{t})d\bar{t}. \tag{13}$$

Numerically, this formula is easily interpreted. The location difference at time t in a step dt is

$$x_1(t + dt) - x_1(t) = v(x_1(t), t)dt. \tag{14}$$

[16] The trajectories for this example are plotted in Figure 3. It is seen that during dilation ($t < \tau$) the velocity of a fluid element is almost constant. After the opening of the veins has ceased, the velocity becomes virtually zero. From
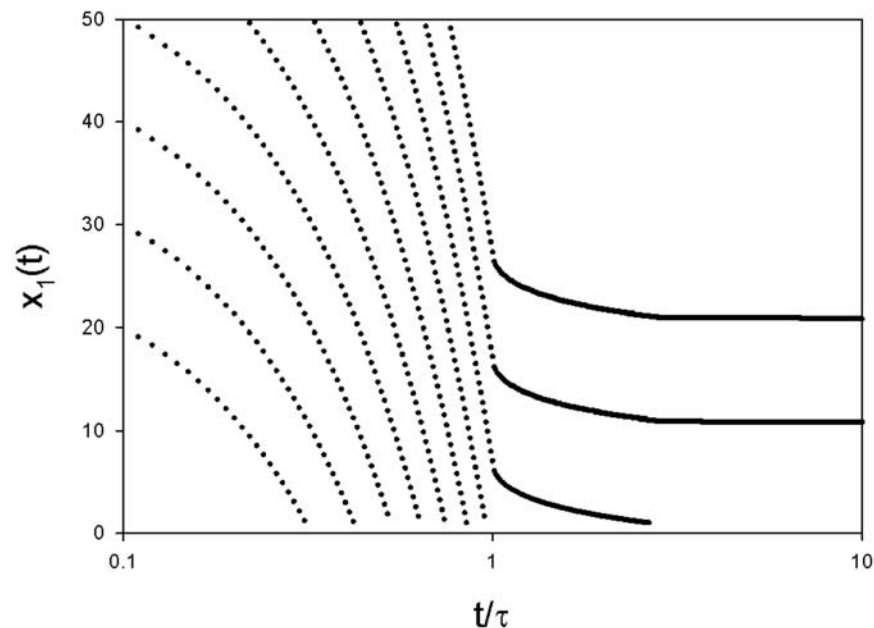

Figure 5. Trajectories as in Figure 4 but with a logarithmic time axis, emphasizing the effect of melt compressibility.

Table 2. Sensitivity Analysis Showing Effects of Changes to Variables Listed in Table 1

Value Other Than Benchmark	Largest Distance (m)	Time to $x = 0$
Value (see Table 1)	100	τ
$\tau = 10^8$ s	100	τ
$\delta = 4$ m	100	1.3τ
$\beta = 10^{-9}$ Pa^{-1}	100	3τ
$k = 10^{-10}$ m^2 Pa^{-1} s^{-1}	100	τ
$k_0 = 10^{-9}$ m^2 Pa^{-1} s^{-1}	100	τ
$e_0 = 0.05$	50	τ
$n = 0.005$	25	1.1τ
$n_0 = 0.4$	100	1.2τ

this, it is concluded that fluid elements that complete their journey toward the central region within the time span $t < \tau$ will arrive in the channelized region, while those that do not complete their journey in this period will not. The trajectories plotted in Figure 3 suggest that for the model parameters listed in Table 1, melt located within a radius of some 100 m of the channel zone will arrive there within the nondimensional timescale ($t/\tau = 1$). The melt flow velocity for this trajectory is $x_1(t)/\tau = 80$ m/3×10^7 s $= 2.5 \times 10^{-6}$ m s^{-1}. A fluid element located 110 m away will not make it to the channel unless the listed variables are changed. Sensitivity analysis suggests that matrix flow is relatively insensitive to matrix permeability.

[17] The same calculation is shown in Figure 4, this time for a melt phase that is slightly more compressible (due to the assumed presence of dissolved volatiles): $\beta = 10^{-9}$ Pa^{-1}. Here it is seen that for $t > \tau$ there is still a small velocity associated with the relaxation of the compressible melt. This would imply that fluid elements that cannot reach the zero region in a time $t < \tau$ may still travel a short distance. A more careful study of this effect is depicted in Figure 5, where the timescale has been stretched by using a logarithmic scale. It is observed that the relaxation effect is confined to trajectories that were already close to the zero region at time $t = \tau$.

[18] A sensitivity analysis is now carried out. Results are given in Table 2. We record the largest distance of a fluid element at time $t = 0$ that arrives at the center of the channel. All parameters are as in Table 1, except for the variation of one that is listed.

5. Discussion

5.1. Comparison With Melt Transport Models Beneath Ridges

[19] For melt extraction in a subduction setting, the matrix downwelling velocity imposes a key timescale. For most subduction zones this is of the order $5-10$ cm a^{-1} (see compilation by *Plank and Langmuir* [1998]). Although decompression melting cannot be ruled out beneath some arcs [*Conder et al.*, 2002], by and large, arc mantle differs significantly from mid-ocean ridges and ocean islands in that the segregation process is coupled with the matrix upwelling velocity [*Stracke et al.*, 2003]. From the analysis given in section 4, the melt flow rate is circa 10^{-6} m s^{-1}, 3 orders of magnitude greater than average downwelling velocity, meaning that over the modeled transport time the matrix is effectively stationary and the model is fixed in the reference frame of the melt. A clear outcome of our analytical calculations under model conditions is that average melt flow velocities lie at the upper end of those predicted at

constructive plate margins from numerical solutions. Channel formation beneath ridge systems has been modeled successfully using a combination of compaction theory [*McKenzie*, 1985] and reactive fluid flow [e.g., *Spiegelman and Kelemen*, 2003]. However, the estimated timescales for channel formation by reaction infiltration are 10^5 a^{-1}, far too long to preserve the observed U series disequilibria in arc magmas. Our melt transport model differs fundamentally from these and most other treatments (with the notable exception of that of *Ribe* [1986]) in that it deals with the lateral flow of melt, for which evidence exists from field studies of ophiolite complexes [e.g., *Abelson et al.*, 2001]. As we are not promoting buoyancy-driven flow, melt drawn into an opening channel is in principle free to flow toward it from any direction. On the basis of the illustrative values and constants listed in Table 1, the zone of influence surrounding a 2-m-wide dilating channel structure is 80 m. Keeping with this simple example but extending now to three dimensions, a volume $\sim 2 \times 10^9$ L of mantle rock could, in principle, be sampled by percolating melt moving toward a dilating channel on a characteristic timescale of 1 year. This is several times larger than the typical volumetric melting rate beneath arcs of 3×10^{-4} km^3 a^{-1}, implying that the sucking effect could operate on length scales that are significant with respect to typical magma production rates. The potential sample volume will be clearly larger if the model timescale (τ) is increased. Should the source region comprise numerous, closely spaced channels (similar arrangements beneath mid-ocean ridges suggest spacings of a meter to several hundred meters [*Kelemen and Dick*, 1995]), then conceptually we can imagine a situation where melt is sucked toward channels which have overlapping radii of influence. Should the mantle wedge be chemically heterogeneous on a scale comparable with the melt transport distance, governed largely by the channel opening rate, the opportunity exists to impart chemical variation in the melt phase at source as it migrates toward and into a dilating channel. While a full exploration of the geochemical consequences on melt composition entering a channel lie outside the scope of this study, it should be noted that lateral flow has the potential to introduce subtle and potentially complex chemical variations in trace element and isotopic compositions of melts in the source region that may not be apparent in models based purely on gravity-driven flow.

5.2. Speculations on Channel Formation in Downwelling Mantle Wedge

[20] Implicit in the modeling is that channels with individually dilating veins can actually form in the source region. But how might this happen in reality? Arguably, there should be some link between partial melting and channel formation (similar arguments hold sway in the continental crust [see *Brown and Rushmer*, 1997, and references therein]), but this link is not obvious in mantle rocks. For example, while partial melting has been shown to result in volume changes sufficient in magnitude to induce cracking in ductile media [*Rushmer*, 2001], the general outcome of this process is to push fluid out of the rock [e.g., *Murton et al.*, 2006] not to suck it in as argued here. It, thus, seems that thermal stresses associated with partial melting are unlikely to be the primary cause of dilation in this instance.

[21] The alternative is to appeal to tectonic deformation. It has been noted that the interface between the downwelling slab and overriding mantle wedge is a type of shear zone [e.g., *van Keken*, 2003] resulting in localized, high-temperature viscous deformation. If an elliptical object is simply sheared with shear strain γ, the volume strain is of the order of γ^2. This direct "mean field" approach would imply that the volume strain rate is a second-order effect. This is not so when an inclusion-type theory for elliptical inclusions in an elastic medium (ideal mantle matrix) is considered. Formulas for this are available [*Walpole*, 1977]. Here no full calculations are given, but if the formulae are made relevant to an elliptical channel aligned with major principal direction of the shear direction, the volume strain is of the order of magnitude of the shear strain γ for a channel in which the major principal axis is much greater than the minor principal axis. Thus, it follows that the rate of shear required to drive the process envisaged here must be of the order of magnitude of 10^{-7} s^{-1} if the zone marked zero (Figure 1) has a vein concentration of some 10%. Such a rate of shearing is clearly much larger than the mean tectonic background value. The tentative implication is that during subduction, localized zones of dilation leading to channel formation will only occur at higher-than-average (plate tectonic) strain rates. However, the model still requires that melting, or a melt phase, is located within sucking distance of an opening channel. In standard iso-viscous mantle models, the zone of partial melting is restricted to a confined region located above and away from the slab top. However, thermal models based on a non-Newtonian rheology focus heat (and by implication partial melting) much closer to the slab mantle interface where viscous deformation is also most likely to be strongest [e.g., *Cagnioncle et al.*, 2007]. Thus, a qualitative picture, underpinned in part by robust physics, emerges whereby channels in the wedge melting zone form because of stresses and draw toward them contemporaneous partial melt from their surroundings as they progressively dilate. Arc mantle with non-Newtonian rheology appears to offer the most convenient way of colocating the essential ingredients of partial melt and shearing in the mantle wedge such that channels of the kind described here can form in the source region.

5.3. Implications for U Series Disequilibria in Arc Magmas

[22] Whatever the finer details of variability in melt composition resulting from radial flow and the mechanism responsible for rapid lithospheric-scale transport of melt to the surface turn out to be, the implications for preserving isotopic disequilibria in arc magmas at source now become clearer. Given the parameters outlined in section 3, small-scale porous flow into veins or channels located in the mantle source region is easily fast enough to preserve excess ^{226}Ra. More controversially, our modeled melt transport times at relevant melt fractions (10^{-3}) are less than the ^{210}Pb half-life of 22.5 years. This raises the theoretical possibility that some ^{210}Pb deficits in arc lavas reflect fractionation during partial melting rather than late stage contrasts in gas and magma transport beneath the volcanic edifice [*Turner et al.*, 2004]. A similar conclusion was reached by *Rubin et al.* [2005b], who used ^{210}Pb deficits in mid-ocean ridge basalts to argue for ultrarapid

melt extraction rates of less than a decade. Our results suggest that lateral porous media flow on the decimeter scale, driven by relatively modest pressure gradients, is consistent with the idea that short-lived isotope disequilibria in some arc magmas would derive from melting at source.

[23] In the arc environment this is, in principle, testable by obtaining further ^{210}Pb data on primitive lavas and looking for correlations with indices of fluid addition or other melting signals such as ^{235}U-^{231}Pa disequilibria. Moreover, if ^{231}Pa-^{227}Ac disequilibria were found in arc lavas, this would prove that melting-induced disequilibria formed on the decadal timescale can be preserved since unlike ^{226}Ra-^{210}Pb, there is no gaseous intermediate in this system to offer an alternative explanation. While both of these tests must await further data collection, it is worthwhile considering the ramifications of these timescales for melt segregation if applicable. The most obvious is that measured ^{226}Ra excesses would be primary and unaffected by decay in any lavas shown to preserve a source ^{210}Pb (or ^{227}Ac) signal. First, ^{230}Th-^{226}Ra disequilibria is primarily a function of residual porosity in the melting region, and this could, in principle, be quantified, removing a key unknown in all ingrowth melting models. Second, as ^{226}Ra excesses are frequently thought to derive from the base of the arc melting column, tighter constraints on melt ascent would be possible, and these may rule out models invoking significant melt–wall rock interaction during magma passage. Third, the commonly observed decreases in (^{226}Ra/^{230}Th) with increasing extent of differentiation would no longer constrain the timescales of differentiation but rather would require a major role for amphibole during fractionation. Evidence for this has been emerging [*Davidson et al.*, 2007]. Instead, differentiation would have to occur on the decadal timescale and, thus, be similar to eruptive periodicity. This might reconcile some very young ages from diffusion studies (see review by *Turner and Costa* [2007]) and would require that differentiation occur during magma ascent and be strongly controlled by decompression [e.g., *Blundy and Cashman*, 2001] rather than just crystallization due to cooling alone.

Appendix A

[24] Three regions are distinguished (Figure 1): zero, where the veins comprising the high-permeability channel are located; plus, almost undeformable permeable material to the right of zero at $x > \delta$; and minus, almost undeformable permeable material to the left of 0 at $x < -\delta$. The flow is driven by a strain that is ramped up to a value e_0 in a time τ. For $t > \tau$ the strain is constant at e_0.

[25] Biot's equation reads

$$k_0 \frac{\partial^2 p}{\partial x^2} = n_0 \beta \frac{\partial p}{\partial t} + \frac{\partial e}{\partial t} \quad (-\delta < x < \delta) \tag{A1}$$

$$k \frac{\partial^2 p}{\partial x^2} = n\beta \frac{\partial p}{\partial t} \quad (x > \delta, \ x < -\delta). \tag{A2}$$

[26] The boundary conditions are

$$p(\delta - \varepsilon, t) = p(\delta + \varepsilon, t) \quad (\varepsilon \to 0), \tag{A3}$$

$$p(-\delta - \varepsilon, t) = p(-\delta + \varepsilon, t) \quad (\varepsilon \to 0), \tag{A4}$$

$$k_0 \frac{\partial p}{\partial x}(\delta - \varepsilon, t) = k \frac{\partial p}{\partial x}(\delta + \varepsilon, t) \quad (\varepsilon \to 0), \qquad (A5)$$

$$k_0 \frac{\partial p}{\partial x}(-\delta + \varepsilon, t) = k \frac{\partial p}{\partial x}(-\delta - \varepsilon, t) \quad (\varepsilon \to 0), \qquad (A6)$$

$$\frac{\partial p}{\partial x}(\pm L, t) = 0 \quad (L \to \infty). \qquad (A7)$$

[27] The solution is obtained by Laplace transform with Laplace frequency s:

$$k_0 \frac{\partial^2 \widehat{p}}{\partial x^2} = n_0 \beta s \widehat{p} + s \widehat{e} \quad (-\delta < x < \delta) \qquad (A8)$$

$$k \frac{\partial^2 \widehat{p}}{\partial x^2} = n \beta s \widehat{p} \quad (x > \delta, \; x < -\delta). \qquad (A9)$$

[28] The solution is for the minus region,

$$\widehat{p} = \frac{\widehat{e} k_0 \mu_0 e^{\mu(x+\delta)\sqrt{s}}\left(1 - e^{2\mu_0\delta\sqrt{s}}\right)}{\beta n_0 \left(e^{2\mu_0\delta\sqrt{s}}(k\mu + k_0\mu_0) + k\mu - k_0\mu_0\right)}, \qquad (A10)$$

zero region,

$$\widehat{p} = \frac{\widehat{e} k\mu \left[e^{\mu_0(x+\delta)\sqrt{s}} + e^{\mu_0(-x+\delta)\sqrt{s}}\right]}{\beta n_0 \left(e^{2\mu_0\delta\sqrt{s}}(k\mu + k_0\mu_0) + k\mu - k_0\mu_0\right)}, \qquad (A11)$$

and plus region,

$$\widehat{p} = \frac{\widehat{e} k_0 \mu_0 e^{\mu(-x+\delta)\sqrt{s}}\left(1 - e^{2\mu_0\delta\sqrt{s}}\right)}{\beta n_0 \left(e^{2\mu_0\delta\sqrt{s}}(k\mu + k_0\mu_0) + k\mu - k_0\mu_0\right)}, \qquad (A12)$$

where $\mu_0 = \sqrt{n_0\beta/k_0}$ and $\mu = \sqrt{n\beta/k}$.

[29] The superficial velocity is obtained from

$$v = -k\frac{\partial p}{\partial x}. \qquad (A13)$$

So, the minus region is

$$\widehat{v} = -\frac{\widehat{e} k k_0 \mu_0 \mu \sqrt{s} e^{\mu(x+\delta)\sqrt{s}}\left(1 - e^{2\mu_0\delta\sqrt{s}}\right)}{\beta n_0 \left(e^{2\mu_0\delta\sqrt{s}}(k\mu + k_0\mu_0) + k\mu - k_0\mu_0\right)}, \qquad (A14)$$

zero region is

$$\widehat{v} = \frac{\widehat{e} k^2 \mu \sqrt{s}\left[\mu_0 e^{\mu_0(x+\delta)\sqrt{s}} - e^{\mu_0(-x+\delta)\sqrt{s}}\right]}{\beta n_0 \left(e^{2\mu_0\delta\sqrt{s}}(k\mu + k_0\mu_0) + k\mu - k_0\mu_0\right)}, \qquad (A15)$$

and plus region is

$$\widehat{v} = \frac{\widehat{e} k k_0 \mu_0 \mu \sqrt{s} e^{\mu(-x+\delta)\sqrt{s}}\left(1 - e^{2\mu_0\delta\sqrt{s}}\right)}{\beta n_0 \left(e^{2\mu_0\delta\sqrt{s}}(k\mu + k_0\mu_0) + k\mu - k_0\mu_0\right)}. \qquad (A16)$$

A1. Solution in the Plus Region

[30] The inverse Laplace transform in the plus region is obtained as follows:

$$\widehat{e}\frac{k_0\mu_0}{\beta n_0(k\mu + k_0\mu_0)} \frac{e^{\mu(-x+\delta)\sqrt{s}}\left(e^{-2\mu_0\delta\sqrt{s}} - 1\right)}{\left(1 + \frac{k\mu - k_0\mu_0}{k\mu + k_0\mu_0}e^{-2\mu_0\delta\sqrt{s}}\right)}$$

$$= \widehat{e}\frac{k_0\mu_0 e^{\mu(-x+\delta)\sqrt{s}}\left(e^{-2\mu_0\delta\sqrt{s}} - 1\right)}{\beta n_0(k\mu + k_0\mu_0)} \sum_{j=0}^{\infty} \left(\frac{-k\mu + k_0\mu_0}{k\mu + k_0\mu_0}\right)^j e^{-2j\mu_0\delta\sqrt{s}}.$$

[31] Now, a slightly more general approach is taken. First, note that

$$\text{\textsterling}^{-1}\left(e^{-\zeta\sqrt{s}}\right) = \frac{\zeta}{2\sqrt{\pi t^3}}e^{-\zeta^2/(4t)}$$

and

$$\text{\textsterling}^{-1}(\widehat{e}) = e_0\frac{t}{\tau} \quad (t < \tau) \; = e_0 \quad (t > \tau), \qquad (A17)$$

so,

$$\text{\textsterling}^{-1}\left(\widehat{e}e^{-\zeta\sqrt{s}}\right) = \int_0^t e_0 \frac{(t - \lambda)}{\tau}\frac{\zeta}{2\sqrt{\pi\lambda^3}}e^{-\zeta^2/(4\lambda)} \quad (t < \tau)$$

$$= \int_{t-\tau}^t e_0 \frac{(t - \lambda)}{\tau}\frac{\zeta}{2\sqrt{\pi\lambda^3}}e^{-\zeta^2/(4\lambda)}$$

$$+ \int_0^{t-\tau} e_0 \frac{\zeta}{2\sqrt{\pi\lambda^3}}e^{-\zeta^2/(4\lambda)} \quad (t > \tau). \qquad (A18)$$

[32] The integrals are easily done, and the outcome is

$$\text{\textsterling}^{-1}\left(\widehat{e}e^{-\zeta\sqrt{s}}\right)$$

$$= -\frac{e_0\zeta\sqrt{t}\exp\left(-\frac{\zeta^2}{4t}\right)}{\tau\sqrt{\pi}} + \frac{e_0(2t + \zeta^2)\left[1 - \mathrm{erf}\left(\frac{\zeta}{2\sqrt{t}}\right)\right]}{2\tau} \quad (t < \tau)$$

$$= e_0 + \frac{e_0\zeta\left(\exp\left(\frac{-\zeta^2}{4(t-\tau)}\right)\sqrt{t-\tau} - \exp\left(\frac{-\zeta^2}{4t}\right)\sqrt{t}\right)}{\tau\sqrt{\pi}}$$

$$\cdot \frac{e_0\left[(2t - 2\tau + \zeta^2)\mathrm{erf}\left(\frac{\zeta}{2\sqrt{t-\tau}}\right) - (2t + \zeta^2)\mathrm{erf}\left(\frac{\zeta}{2\sqrt{t}}\right)\right]}{2\tau}$$

$$\cdot (t > \tau). \qquad (A19)$$

[33] Call $\widehat{\Psi}_0 e_0 \equiv \text{\textsterling}^{-1}(\widehat{e}e^{-\zeta\sqrt{s}})$, then the following hierarchy is generated:

$$\widehat{\Psi}_1(s, \zeta)e_0 = \text{\textsterling}^{-1}\left(\widehat{e}\sqrt{s}e^{-\zeta\sqrt{s}}\right) = -\frac{\partial}{\partial\zeta}\text{\textsterling}^{-1}\left(\widehat{e}e^{-\zeta\sqrt{s}}\right),$$

$$\widehat{\Psi}_2(s, \zeta)e_0 = \text{\textsterling}^{-1}\left(\widehat{e}s e^{-\zeta\sqrt{s}}\right) = \frac{\partial^2}{\partial\zeta^2}\text{\textsterling}^{-1}\left(\widehat{e}e^{-\zeta\sqrt{s}}\right), \qquad (A20)$$

etc.

[34] In the time domain, the differentiations with respect to ζ yield the following:

$$\Psi_1(\zeta,t) = \frac{2\sqrt{t}\exp\left(-\frac{\zeta^2}{4t}\right)}{\tau\sqrt{\pi}} - \frac{\zeta\left[1 - \operatorname{erf}\left(\frac{\zeta}{2\sqrt{t}}\right)\right]}{\tau} \quad (t < \tau)$$

$$= -\frac{2\left(\exp\left(\frac{-\zeta^2}{4(t-\tau)}\right)\sqrt{t-\tau} - \exp\left(\frac{-\zeta^2}{4t}\right)\sqrt{t}\right)}{\tau\sqrt{\pi}}$$

$$- \frac{\zeta\left[\operatorname{erf}\left(\frac{\zeta}{2\sqrt{t-\tau}}\right) - \operatorname{erf}\left(\frac{\zeta}{2\sqrt{t}}\right)\right]}{\tau} \quad (t > \tau), \quad (A21)$$

$$\Psi_2(\zeta,t) = \frac{\zeta\left[1 - \operatorname{erf}\left(\frac{\zeta}{2\sqrt{t}}\right)\right]}{\tau} \quad (t < \tau)$$

$$= \frac{\zeta\left[\operatorname{erf}\left(\frac{\zeta}{2\sqrt{t-\tau}}\right) - \operatorname{erf}\left(\frac{\zeta}{2\sqrt{t}}\right)\right]}{\tau} \quad (t > \tau), \quad (A22)$$

$$\Psi_3(\zeta,t) = \frac{\exp\left(-\frac{\zeta^2}{4t}\right)}{\tau\sqrt{\pi t}} \quad (t < \tau)$$

$$= \frac{\exp\left(\frac{-\zeta^2}{4t}\right)}{\tau\sqrt{\pi t}} - \frac{\exp\left(\frac{-\zeta^2}{4(t-\tau)}\right)}{\tau\sqrt{\pi(t-\tau)}} \quad (t > \tau), \quad (A23)$$

$$p(x,t) = \frac{e_0 k_0 \mu_0}{\beta n_0 (k\mu + k_0\mu_0)} \sum_{j=0}^{\infty} \left(\frac{-k\mu + k_0\mu_0}{k\mu + k_0\mu_0}\right)^j$$

$$\cdot \left[\Psi_0(\mu(x-\delta) + 2(j+1)\mu_0\delta, t)\right.$$

$$\left. - \Psi_0(\mu(x-\delta) + 2j\mu_0\delta, t)\right], \quad (A24)$$

$$v(x,t) = -\frac{e_0 k k_0 \mu_0 \mu}{\beta n_0 (k\mu + k_0\mu_0)} \sum_{j=0}^{\infty} \left(\frac{-k\mu + k_0\mu_0}{k\mu + k_0\mu_0}\right)^j$$

$$\cdot \left[\Psi_1(\mu(x-\delta) + 2(j+1)\mu_0\delta, t)\right.$$

$$\left. - \Psi_1(\mu(x-\delta) + 2j\mu_0\delta, t)\right]. \quad (A25)$$

A2. Long Time Approximation

[35] For long times, that is for $t \gg 4(\mu_0\delta)^2$, the formulas may be approximated. In the plus region,

$$\widehat{p} = \widehat{e}e^{\mu(-x+\delta)\sqrt{s}}\left(\frac{\delta\sqrt{s}}{\sqrt{\beta nk}} - \frac{\delta^2 n_0 s}{nk}\right), \quad (A26)$$

$$\widehat{v} = \widehat{e}e^{\mu(-x+\delta)\sqrt{s}}\left(-\delta s + \delta^2 n_0 s^{3/2}\sqrt{\frac{\beta}{nk}}\right). \quad (A27)$$

In the time domain, these become

$$p(x,t) = -\frac{e_0\delta}{\sqrt{\beta nk}}\Psi_1(\mu(x-\delta), t) + \frac{e_0\delta^2 n_0}{nk}\Psi_2(\mu(x-\delta), t) \quad (A28)$$

$$v(x,t) = -e_0\delta\Psi_2(\mu(x-\delta), t) + e_0\delta^2 n_0\Psi_3(\mu(x-\delta), t). \quad (A29)$$

References

Abelson, M., G. Baer, and A. Agnon (2001), Evidence from gabbro of the Troodos ophiolite for lateral magma transport along a slow-spreading mid-ocean ridge, *Nature*, *409*, 72–75.

Aharonov, E., J. A. Whitehead, P. B. Kelemen, and M. Spiegelman (1995), Channeling instability of upwelling melt in the mantle, *J. Geophys. Res.*, *100*, 20,433–20,450.

Asimow, P. D., and E. M. Stolper (1999), Steady state mantle–melt interactions in one dimension: 1. Equilibrium transport and melt focusing, *J. Petrol.*, *40*, 475–494.

Blundy, J., and K. Cashman (2001), Ascent-driven crystallisation of dacite magmas at Mount St Helens, 1980–1986, *Contrib. Mineral. Petrol.*, *140*, 631–650.

Bourdon, B., S. Turner, and N. M. Ribe (2005), Partial melting and upwelling rates beneath the Azores from a U-series isotope perspective, *Earth Planet. Sci. Lett.*, *239*, 42–56.

Brown, M., and T. Rushmer (1997), The role of deformation in the movement of granitic melt: Views from the laboratory and the field, in *Deformation-Enhanced Fluid Transport in the Earth's Crust and Mantle*, edited by M. B. Holness, pp. 111–139, Chapman and Hall, London.

Cagnioncle, A.-M., E. M. Parmentier, and L. T. Elkins-Tanton (2007), Effect of solid flow above a subducting slab on water distribution and melting at convergent boundaries, *J. Geophys. Res.*, *112*, B09402, doi:10.1029/2007JB004934.

Conder, J. A., D. A. Wiens, and J. Morris (2002), On the decompression melting structure at volcanic arcs and back-arc spreading centers, *Geophys. Res. Lett.*, *29*(15), 1727, doi:10.1029/2002GL015390.

Davidson, J., S. Turner, A. Dosseto, and H. Handley (2007), Amphibole sponge in arc crust?, *Geology*, *35*, 787–790.

Huang, F., and C. C. Lundstrom (2007), ^{231}Pa excesses in arc volcanic rocks: Constraints on melting rates at convergent margins, *Geology*, *35*, 1007–1010.

Kelemen, P. B., and H. J. B. Dick (1995), Focused melt flow and localized deformation in the upper mantle: Juxtaposition of replacive dunite and ductile shear zones in the Josephine peridotite, SW Oregon, *J. Geophys. Res.*, *100*, 423–438.

Maaloe, S. (2005), Extraction of melt from veined mantle source regions during eruptions, *J. Volcanol. Geotherm. Res.*, *147*, 377–390.

McKenzie, D. (1985), ^{230}Th-^{238}U disequilibrium and the melting process beneath ridge axes, *Earth Planet. Sci. Lett.*, *72*, 149–157.

Murton, J. B., R. Peterson, and J.-C. Ozouf (2006), Bedrock fracture by ice segregation in cold regions, *Science*, *314*, 1127–1129.

Plank, T., and C. H. Langmuir (1998), The chemical composition of subducting sediment and its consequences for the crust and mantle, *Chem. Geol.*, *145*, 325–394.

Ribe, N. M. (1986), Melt segregation driven by dynamic forcing, *Geophys. Res. Lett.*, *13*, 1462–1465.

Rubin, K. H., I. van der Zander, M. C. Smith, and E. C. Bergmanis (2005a), ^{210}Pb-^{226}Ra-^{230}Th disequilibria in very young mid-ocean ridge basalts, *Geochim. Cosmochim. Acta*, *69*, A338.

Rubin, K. H., I. van der Zander, M. C. Smith, and E. C. Bergmanis (2005b), New speed limit for ocean ridge magmatism, *Nature*, *437*, 534–538.

Rushmer, T. (2001), Volume change during partial melting reactions: Implications for melt extraction, melt geochemistry and crustal rheology, *Tectonophysics*, *342*, 389–405.

Sleep, N. H. (1988), Tapping melts by veins and dykes, *J. Geophys. Res.*, *93*, 10,225–10,272.

Spiegelman, M., and T. Elliott (1993), Consequences of melt transport for uranium series disequilibrium, *Earth Planet. Sci. Lett.*, *118*, 1–20.

Spiegelman, M., and P. B. Kelemen (2003), Extreme chemical variability as a consequence of channelized melt transport, *Geochem. Geophys. Geosyst.*, *4*(7), 1055, doi:10.1029/2002GC000336.

Spiegelman, M., P. B. Kelemen, and E. Aharonov (2001), Causes and consequences of flow organization during melt transport: The reaction infiltration instability in compactible media, *J. Geophys. Res.*, *106*, 2061–2077.

Stevenson, D. J. (1989), Spontaneous small scale melt segregation in partial melts undergoing deformation, *Geophys. Res. Lett.*, *16*, 1067–1070.

Stracke, A., A. Zindler, V. J. M. Salters, D. McKenzie, and K. Groendvold (2003), The dynamics of melting beneath Theistareykir, northern Iceland, *Geochem. Geophys. Geosyst.*, *4*(10), 8513, doi:10.1029/2002GC000347.

Stracke, A., B. Bourdon, and D. McKenzie (2006), Melt extraction in the Earth's mantle: Constraints from U-Th-Pa-Ra studies in oceanic basalts, *Earth Planet. Sci. Lett.*, *244*, 97–112.

Takahashi, N. (1992), Evidence for melt segregation toward fractures in the Horoman mantle peridotite complex, *Nature*, *359*, 52–55.

Turner, S., and F. Costa (2007), Measuring timescales of magmatic evolution, *Elements*, *3*, 267–273.

Turner, S., P. Evans, and C. Hawkesworth (2001), Ultra-fast source-to-surface movement of melt at island arcs from ^{226}Ra-^{230}Th systematics, *Science*, *292*, 1363–1366.

Turner, S., B. Bourdon, and J. Gill (2003), Insights into magma genesis at convergent margins from U-series isotopes, in *Uranium-Series Geochemistry*, *Rev. Mineral. Geochem.*, vol. 52, edited by B. Bourdon, et al., pp. 255–315., Mineral. Soc. of Am., Washington, D. C.

Turner, S., S. Black, and K. Berlo (2004), ^{210}Pb-^{226}Ra and ^{228}Ra-^{232}Th systematics in young arc lavas: Implications for magma degassing and ascent rates, *Earth Planet. Sci. Lett.*, *227*, 1–16.

Turner, S., M. Regelous, C. Hawkesworth, and K. Rostami (2006), Partial melting processes above subducting plates: Constraints from ^{231}Pa-^{235}U disequilibria, *Geochim. Cosmochim. Acta*, *70*, 480–503.

van Keken, P. E. (2003), The structure and dynamics of the mantle wedge, *Earth Planet. Sci. Lett.*, *215*, 323–338.

Walpole, L. J. (1977), The determination of the elastic field of an ellipsoidal inclusion in an anisotropic medium, *Math. Proc. Cambridge Philos. Soc.*, *81*, 283–289.

Williams, R. W., and J. B. Gill (1989), Effects of partial melting on the uranium decay series, *Geochim. Cosmochim. Acta*, *53*, 1607–1619.

————————————

M. A. Koenders, Centre for Earth and Environmental Science Research, Kingston University, Penrhyn Road, Kingston-upon-Thames KT1 2EE, UK.

N. Petford, School of Conservation Sciences, Bournemouth University, Talbot Campus, Fern Barrow, Poole BH12 5BB, UK. (npetford@bournemouth.ac.uk)

S. Turner, GEMOC, Department of Earth and Planetary Sciences, Macquarie University, Sydney, NSW 2109, Australia.